

Supplement to: Coupling processes and exchange of energy and reactive and non-reactive trace gases at a forest site - results of the EGER experiment

Thomas Foken^{1,g}, Franz X. Meixner^{2,4}, Eva Falge², Cornelius Zetzsch^{3,g}, Andrei Serafimovich^{1,g}, Anika Bargsten², Thomas Behrendt², Tobias Biermann¹, Claudia Breuninger², Stephanie Dix^{1,a}, Tobias Gerken¹, Martina Hunner^{1,a}, Lydia Lehmann-Pape², Korbinian Hens², Georg Jocher^{1,b}, Jürgen Kesselmeier², Johannes Lüers^{1,g}, Jens-Christopher Mayer², Alexander Moravek², Daniel Plake², Michael Riederer¹, Friederike Rütz¹, Monika Scheibe^{2,c}, Lukas Siebicke^{1,d}, Matthias Sörgel³, Katharina Staudt^{1,e}, Ivonne Trebs², Anywhere Tsokankunku², Michael Welling², Veronika Wolff^{2,e}, Zhilin Zhu^{2,f}

[1] {University of Bayreuth, Department of Micrometeorology, D-95440 Bayreuth, Germany}

[2] {Max-Planck-Institute of Chemistry, Biogeochemistry Department, P.O. Box 3060, D-55020 Mainz, Germany}

[3]{University of Bayreuth, Atmospheric Chemistry Research Laboratory, D-95440 Bayreuth, Germany}

[4]{University of Zimbabwe, Department of Physics, P.O. Box MP 167, Mount Pleasant, Harare, Zimbabwe}

[a]{now at: TÜV Süd Industrie Service GmbH Wind Cert Services, Ludwig-Eckert-Straße 10, D- 93049 Regensburg, Germany}

[b] {now at: Alfred-Wegener Institute for Polar and Marine Research, Telegrafenberg A43, D-14473 Potsdam, Germany}

[c] {now at: German Aerospace Center (DLR), Institute of Atmospheric Physics, Münchner Straße 20, D-82234 Oberpfaffenhofen-Wessling}

[d] {now at: Institut national de la recherche agronomique (INRA), BP 709, 97387 Cedex Kourou, French Guiana}

[e] {now at: Agroscope ART Research Station, Reckenholzstrasse 191, CH-8046 Zürich, Switzerland}

[f] {now at: Institute for Geographic Sciences and Natural Resources Research, Chinese Academy of Sciences (CAS), A11 Datun Road, Anwai, Beijing 100101, P.R.China}

[g] {Member of Bayreuth Center of Ecology and Environmental Research (BayCEER), University of Bayreuth, D-95440 Bayreuth, Germany}

Correspondence to: T. Foken (thomas.foken@uni-bayreuth.de)

1. Climate, weather conditions, and concentrations of trace compounds

The *Fichtelgebirge Mountains* are located in the transition zone from maritime to continental climates (Foken, 2003). Since 1994, meteorological data have been monitored at a clearing (*Waldstein-Pflanzgarten*, 50°08'35" N, 11°51'49" E, 765 m a.s.l.) about 200 m west of the *Waldstein-Weidenbrunnen* site. Since 1985 there has also been continuous monitoring of ambient O₃, NO, NO₂ and sulphur dioxide (SO₂) concentrations at the *Waldstein-Pflanzgarten* site (up to 1993 station *Wülfersreuth* of the Bavarian Environment Agency). Since 1985, median annual O₃ concentrations have ranged between 20 and 30 ppb, and median annual NO_x (= NO + NO₂) concentrations between 2 and 5 ppb. Those of sulphur dioxide have, since 1995, been less than 1 ppb (Foken, 2003; Lüers et al., 2009).

Climate data are given in Table S1, complemented by recent climatic trends. While the year 2007 was the warmest in the region since permanent weather observations have started in Bayreuth (1850), the summer 2007 was warm but not extreme. IOP-1 (Table S2), starting just at the end of summer 2007, was always under influence of cyclonic conditions and it was only during the “Golden Days” that the anticyclone “Katrin” dominated Central Europe. From 18 June 2008 onward, IOP-2, in the beginning cold and cyclonic, experienced warmer air (Table S2), which was bordering colder air masses to the north. Under these warm and cyclonic conditions, thunderstorms passed through the *Fichtelgebirge* region including our site on 25 June (8.5 mm, 15:10–16:50 CET). The IOP-2 “Golden Days” period, starting on 28 June, was characterized by dry summer weather, not dominated by an anticyclone, and ended on 03 July with the cyclone “Renate” (44.1 mm of rain). Up to the end of IOP-2 cyclonic conditions (with some showers) returned.

An overview of the meteorological conditions and ambient O₃, NO, NO₂, and SO₂ concentrations is given in Table S3. Wet deposition of the ionic components of rain (in mg m⁻²), integrated over the entire time period of IOP-1 and IOP-2, was found to be typical for the region. Highest wet deposition rates were observed in the rain fall just after the “Golden Days” of IOP-1 and during the heavy rainfall on 03 July, 2008 (IOP-2), respectively. Average O₃, NO, NO₂, and SO₂ concentrations, observed at 31 m (a.gr.) at the main tower were within the typical range of the long-term data (monitored at the *Waldstein-Pflanzgarten* site (3 m a.gr.). During IOP-2, maximum SO₂ and NO₂ concentrations (10.8 ppb and 15.1 ppb, respectively) occurred on 09 June, 2008, when easterly air masses have reached our site from the industrialized regions of the Czech Republic.

Table S1. Climate data for *Waldstein-Pflanzgarten* (period 1971-2000, Foken, 2003) and climate trends (Foken, 2004; Seifert, 2004), *) Classification by Köppen/Trewartha/Rudloff according to Hendl (1991), but Df according classification by Köppen/Geiger (Kottek et al., 2006), **) Fichtelberg-Hüttstadel, 662 m a.s.l.

Parameter	Climate (1971–2000)	Climate trend
height a.s.l.	765 m	
climate zone *	Dc	
annual mean temperature in °C	5.3	0.33 K/10 a, 99 % sign. winter: 0.52 K/10 a, 95 % sign.
annual temperature amplitude in K	18.1	
annual sum of precipitation in mm	1162.5	19 mm/10 a, not significant
month with maximum of precipitation	December, July	
snow cover **	approx. 80 days	–10 days/10 a, 95 % sign.

Table S2. Overview of the meteorological conditions at *Waldstein-Pflanzgarten* site during IOP-1 and IOP-2

Parameter	IOP-1 (6 Sep to 7 Oct 2007)	IOP-2 (1 Jun to 15 Jul 2008)
mean temperature in °C relation to normal	9.9 °C Sep too cold (t1.2 K); Oct too cold (t0.6 K)	15.2 °C Jun too warm (+1.5 K); Jul normal (+0.2 K)
absolute maximum temperature in °C	21.0 °C at 24 Sep 2007	28.9 °C at 22 Jun 2008
absolute minimum temperature in °C	2.8 °C at 19 Sep 2007	3.7 °C at 14 Jun 2008
precipitation sum in mm relation to normal	113.2 mm Sep too wet, from 30 Sep no rain; Oct to dry.	112.8 mm Jun too dry, no rain from 18 Jun to 3 Jul except a thunderstorm at 25 Jun 2008; Jul normal
maximum daily sum precipitation in mm	22.1 mm at 27 Sep 2007	44.1 mm at 3 Jul 2008
mean incoming shortwave radiation in $W m^{-2}$ (24 h)	80.4 $W m^{-2}$	225.6 $W m^{-2}$
maximum daily mean incoming shortwave radiation in $W m^{-2}$	152.5 $W m^{-2}$ 15 Sep 2007	at 342.7 $W m^{-2}$ at 1 Jun 2008

Table S3. Overview of trace gas concentrations (ppb) and total of wet deposition (ionic components; mg m^{-2}) during the Intensive Observation Periods of the EGER project (IOP-1, IOP-2), measured at the *Waldstein-Weidenbrunnen* site (31 m a.gr.) and *Waldstein-Pflanzgarten* site (wet deposition, 1.5 m a.gr.), respectively.

Trace gas	IOP-1 6 Sep–3 Oct 2007	IOP-2 1 Jun–11 Jul 2008
ozone (O_3)	33 ppb (average) 50 ppb (95 % quantile)	55 ppb (average) 76 ppb (95 % quantile)
maximum O_3	59 ppb (23 Sep 2007)	85 ppb (6 Jun 2008)
nitric oxide (NO)	0.3 ppb (average) 1.1 ppb (95 % quantile)	0.2 ppb (average) 0.6 ppb (95 % quantile)
maximum NO	2.5 ppb at (2 Oct 2007)	3.4 ppb (7 Jun 2008)
nitrogen dioxide (NO_2)	3.1 ppb (average) 6.7 ppb (95 % quantile)	2.5 ppb (average) 4.6 ppb (95 % quantile)
maximum NO_2	28.5 ppb (28 Sep 2007)	15.6 ppb (9 Jun 2008)
sulphur dioxide (SO_2)	N/A	0.8 ppb (mean) 2.6 ppb (95 % quantile)
maximum SO_2	N/A	10.8 ppb (9 Jun 2008)
total of wet deposition (ionic components)	IOP-1	IOP-2
Cl^-	55 mg m^{-2}	$< 22 \text{ mg m}^{-2}$
NO_2^-	$< 7 \text{ mg m}^{-2}$	$< 4 \text{ mg m}^{-2}$
NO_3^-	297 mg m^{-2}	187 mg m^{-2}
SO_4^{2-}	199 mg m^{-2}	114 mg m^{-2}
NH_4^+	107 mg m^{-2}	78 mg m^{-2}
K^+	$< 30 \text{ mg m}^{-2}$	$< 18 \text{ mg m}^{-2}$
Mg^{2+}	5 mg m^{-2}	$< 6 \text{ mg m}^{-2}$
Ca^{2+}	32 mg m^{-2}	36 mg m^{-2}

2. Additional information about the experimental set up

The locations of the installed towers of the EGER experiment are shown in Fig. S1; exact geographical positions of all towers and remote sensing instruments are listed in Tables S4 and S5, respectively. The footprint climatology of the entire year 2003 of the *Waldstein-Weidenbrunnen* site (see Siebicke 2008) is shown in Fig. S2. Clear cuts performed during the planning period of EGER, the wind-throws (and following clear cuts) after the storms “Ky-rill” (18 January, 2007) and “Emma” (01 March, 2008) had somewhat, but insignificantly affected the footprint distribution of 2003 in the SW corner of the map (not shown).



Figure S1. Towers at the *Waldstein-Weidenbrunnen* site: left: Permanent main tower since 1996 (height 31 m) for routine measurements, FLUXNET station and chemical measurements, middle: turbulence tower (height 35 m) since 2007 with second FLUXNET complex and turbulence measurements, right: biological tower (height 36 m) for gas exchange measurements at needles.

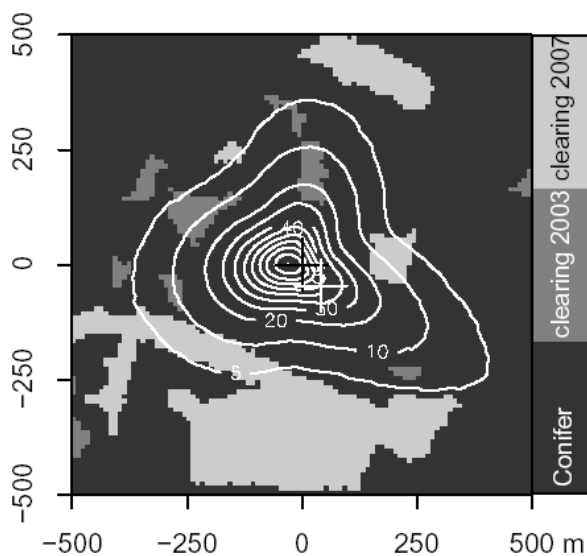


Figure S2. Footprint climatology (for the year 2003) of the *Waldstein-Weidenbrunnen* site (details, see text). Black and white crosses indicate positions of the main and turbulence towers, respectively, while white contour lines are relative flux contributions (in %) to the footprint (Siebicke, 2008).

Table S4. Towers at the Waldstein-Weidenbrunnen site during the Intensive Observation Periods of the EGER project (IOP-1: 2007; IOP-2: 2008)

	Coordinates	Height [m]	Major equipment
"main tower"	50°08'31.2" N 11°52'00.8" E 775 m a.s.l.	31	FLUXNET station Wind-, dry and wet bulb temperature profiles Profiles of trace gas concentrations and fluxes Measurements of soil related quantities and trace gas soil flux measurements (dynamic chambers), within a radius of 10–50 m
"turbulence tower"	50°08'29.9" N 11°52'03.1" E	35	Profile of turbulent energy and carbon dioxide fluxes
"bio-tower"	50°08'32.9" N 11°51'57.8" E	36	Vertical profile of sapflow, temperature, humidity, and net radiation CO ₂ and H ₂ O exchange measurements on spruce branches (dynamic cuvette)

Table S5. Remote sensing techniques used during the Intensive Observation Periods of the EGER project (IOP-1: 2007; IOP-2: 2008)

Device	Coordinates	Location
2-D sonic anemometer (Thies)	50°08'31.2" N, 11°52'00.8" E 775 m a.s.l. + 32 m	Waldstein-Weidenbrunnen, „main tower“
mini-sodar, SFAS (Scintec AG)	50°08'30.3" N, 11°52'11.0" E 785 m a.s.l.	clearing, NE of Waldstein-Weidenbrunnen site
Sodar/RASS, DSDPA90.64 (METEK GmbH)	50°08'35.3" N, 11°51'48.8" E 764 m a.s.l.	Waldstein-Pflanzgarten
UHF-windprofiler (Vaisala)	49.98° N, 11.68° E 514 m a.s.l.	Oschenberg near Bayreuth

3. Characteristic turbulent and chemical time scales; Damköhler numbers of the NO-NO₂-O₃ triad

The Damköhler number (DA) is the ratio of two particular time scales, namely the characteristic turbulent transport time (τ_{turb}) over the characteristic chemical time scale (τ_{chem}):

$$DA = \frac{\tau_{turb}}{\tau_{chem}} \quad (S1)$$

Dominance of the turbulent transport over chemical reaction (hence, treating a trace substance as “non-reactive” during transport through the forest or considering a trace substance as “non-reactive” for “volume averaging”) is given, if $DA \leq 0.1$. Defined by the K-approach, the cha-

racteristic turbulent time scale, τ_{turb} , may be computed from the mean transfer velocity v_t and the thickness Δz of the layer being considered (Mayer et al., 2011)

$$\tau_{turb} = \frac{\Delta z}{v_t} \quad (S2)$$

The final expression for the time scales of turbulent trace gas transport thus reads:

$$\tau_{turb} = \frac{\Delta z^2 \cdot \varphi_H(\zeta) \cdot Sc_t}{\kappa \cdot z_m \cdot u_*} \quad (S3)$$

with φ_H the universal function for the heat exchange (also used for trace gases), $\zeta=z/L$ with the Obukhov-length L , the von-Kármán-constant κ , the measuring height z_m , the turbulent Schmidt number Sc_t , and the friction velocity u_* . It should be stated that Eq. (S3) is only applicable under Monin-Obukhov similarity conditions.

Typical time scales for reactions of chemically reactive compounds are given in Appendix B (reactions 1-15, see Dlugi, 1993). However, assuming reasonable vertical mixing and considering given (measured) concentrations of reaction partners, the characteristic chemical reaction times can be calculated using (i) kinetic constants (Atkinson et al., 2004), (ii) radiation fluxes for photolysis (e.g. for O_3 , NO_2 , and HONO), and (iii) known thermodynamic quantities, NH_3 - HNO_3 - NH_4NO_3 , (see Wolff et al., 2010b), respectively. As Mayer et al. (2011), we consider for the chemical timescale (τ_{chem}) only the NO- NO_2 - O_3 triad comprising the reactions $O_3 + NO \rightarrow NO_2 + O_2$ (reaction coefficient $k_1 = 1.40 \times 10^{-12} \exp^{-1310/T}$ (see Atkinson et al., 2004) and $NO_2 + h\nu \rightarrow NO + O_3$ ($\lambda < 420\text{nm}$), characterized by the NO_2 photolysis frequency $j(NO_2)$, which has been measured directly. Destruction of NO_2 is then controlled by $j(NO_2)$ only and, in turn, the chemical production of NO and O_3 . From simple reaction kinetics, the time scales for NO, NO_2 and O_3 are given by $\tau_{NO} = (k_1 N_{O_3})^{-1}$, $\tau_{NO_2} = (j(NO_2))^{-1}$, and $\tau_{O_3} = (k_1 N_{NO})^{-1}$ (where N_{NO} and N_{O_3} represent the molecule number density of NO and O_3). The overall chemical timescale of the NO- NO_2 - O_3 triad (τ_{chem}), a measure of the extent of chemical conversions (for comparison with the turbulent time scale τ_{turb}), has been formulated by Lenschow (1982):

$$\tau_{chem} = \frac{2}{\sqrt{(j(NO_2))^2 + k_1^2 (N_{O_3} - N_{NO}) + 2k_1 j(NO_2) (N_{O_3} + N_{NO} + 2N_{NO_2})}} \quad (S4)$$

4. Flux-gradient relations and roughness sub-layer

Because of the substantially enhanced aerodynamic roughness of the forest canopy in comparison to smooth surfaces, where the Monin-Obukhov similarity theory is valid, a stronger mixing occurs over forest canopies (mixing layer theory, see Sect. 1 and 2.4). Consequently, higher fluxes will occur in case of lower gradients. This can be compensated by application of an universal function φ_* of the roughness sub-layer (of thickness z_*). From integration of flux-gradient equations between two levels follows the aerodynamic method for the trace gas flux (Foken, 2008a; Monteith and Unsworth, 2008).

The profile function for scalars and momentum in the integrated form is given by

$$F_c = -\frac{\kappa^2 (u_2 - u_1)(c_2 - c_1)}{\{\ln[(z_2 - d)/(z_1 - d)]\}^2} (\Phi_m \Phi_c)^{-1} \quad (\text{S5})$$

This equation was already formulated for the application above a canopy with the zero-plane displacement height d . According to the definition of the profile functions in the roughness sub-layer the universal function of the roughness sub-layer φ_* must be included. The site specific universal functions of the roughness sub-layer is called enhancement factor. The enhancement factor for scalars was often assumed to be $1/\varphi_{c*}(z/z_*) \approx 1$. Instead of using an enhancement factor for momentum, the friction velocity is often directly determined with eddy-covariance measurements at the relevant height of the application of the aerodynamic method. With this assumption it follows for Eq. (S5)

$$F_c = \overline{w'c'} = -\frac{\kappa u_* (c_2 - c_1)}{\ln[(z_2 - d)/(z_1 - d)]} \Phi_c^{-1}. \quad (\text{S6})$$

Therefore, an unknown error due to the enhancement factor for scalars must be assumed which underestimates the fluxes up to 30-60 %, if the enhancement factor for scalars is in the same order as that for the momentum exchange (Mölder et al., 1999).

The usual procedure to characterize the roughness sub-layer could not be realized for the *Waldstein-Weidenbrunnen* site, simply because none of the EGER towers was tall enough to install a sufficient number of measurement levels between the top of the canopy (23-25 m a.gr.) and the roughness sub-layer height z_* (presumably >50 m a.gr.). Data from the sodar/RASS and the mini-sodar cannot be used because their (large) footprint is not representative for the *Waldstein-Weidenbrunnen* forest. Therefore, we preferred using the following alternative to derive the desired correction function $\varphi_*(z/z_*)$. The function φ_* has been deter-

mined from data obtained during the recent field experiment COPS (Wulfmeyer et al., 2011), performed over a growing maize field (for details see Eigenmann et al., 2009).

In Fig. S3 the results of the COPS experiment over maize are shown in comparison with the data from the Waldstein-Weidenbrunnen site (only in the range $z/z_*=0.41 - 0.45$) and the equations

$$\varphi_*(z/z_*) = \exp[-0.7(1 - z/z_*)] \quad (\text{S7})$$

(Garratt, 1992) and

$$\varphi_{*u} = \left(\frac{z}{z_*}\right)^\eta \quad (\text{S8})$$

(Cellier and Brunet, 1992). A strong dependence on the friction velocity was found, but for moderate friction velocities up to 0.6 m s^{-1} , Eq. (S8) gives the best approximation with $\eta=0.6$, which was also found by Mölder et al. (1999). A slight but not significant dependence on stability was also recognised. The enhancement factor for the momentum exchange at 31 m height is therefore approximately 1.6.

Similar to other authors (Mölder et al., 1999), the number of measuring points and the accuracy of the data were not adequate for the calculation of the universal function of the roughness sub-layer for scalars. For the temperature profile over the maize field the linear relationship with $\eta=1.0$ was in agreement with Mölder et al. (1999). At the forest site the scalars at a height of 23 m, at the top of the canopy, already showed an increased gradient to the top of the tower and no reduced gradient according to the roughness sub-layer assumption. Therefore, for scalars no additional enhancement factor should be used.

For many trace gases the use of the eddy-covariance technique is not yet feasible due to the lack of fast response sensors. The aerodynamic method, as described above, was not directly applied in the present paper, but in parallel studies (Wolff et al., 2010a; Wolff et al., 2010b); furthermore, the site specific enhancement factor is important for the interpretation of fluxes and gradients (see Sect. 3.5). Moreover, characteristics of the roughness sub-layer are relevant for the mixing layer theory, which is the basis for the coupling approach (see Sect. 2.4)

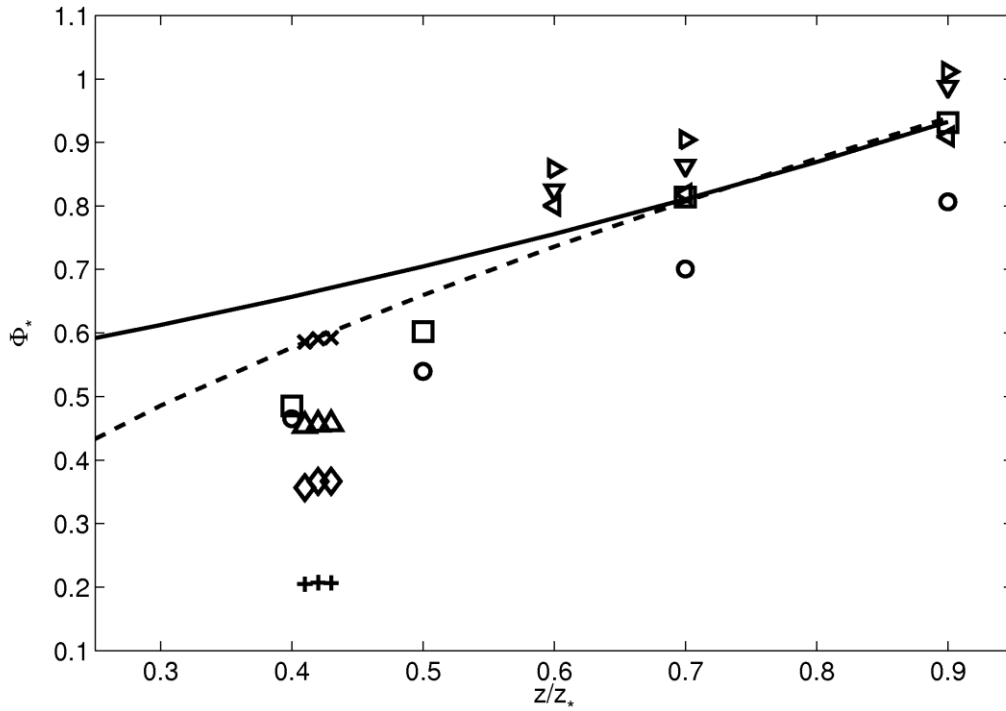


Figure S3. The calculated ϕ_* values of the EGER data are presented by crosses, upward-pointing triangles, diamonds, and plus signs. The crosses represent u_* values smaller than 0.4 and larger than 0.2. Further the upward-pointing triangles represent $0.4 < u_* < 0.6$, the diamonds $0.6 < u_* < 0.8$ and the plus signs $0.8 < u_* < 1.2$. The calculated ϕ_* values of the COPS data for a canopy height of 1.2m are represented by squares and circles. The squares represent $0.2 < u_* < 0.3$ and the circles represent $0.3 < u_* < 0.6$. The calculated ϕ_* values of the COPS data for a canopy height of 2.9m are represented by downward-pointing, right-pointing, and left-pointing triangles. The downward-pointing triangles represent $0.2 < u_* < 0.3$, the right-pointing triangles display $0.3 < u_* < 0.4$ and left-pointing triangles $0.4 < u_* < 0.5$. Furthermore, the solid line represents the equation developed by Garratt (1992) and the dashed line represents the equation developed by Mölder et al. (1999).

5. Energy balance closure

In former studies (Aubinet et al., 2000; Foken, 2008b), a value of 77 % for the energy balance closure was found according to

$$100 - \text{Re}_s[\%] = \frac{H + LE + G}{R_n} \cdot 100\% \quad (\text{S9})$$

with the net radiation R_n , the sensible heat flux H , the latent heat flux LE , the ground heat flux G , and residual of the energy balance closure Res . In this study the heat storage was neglected. During both IOPs similar values were found with approx. 80 % for both IOP's (Fig. S4).

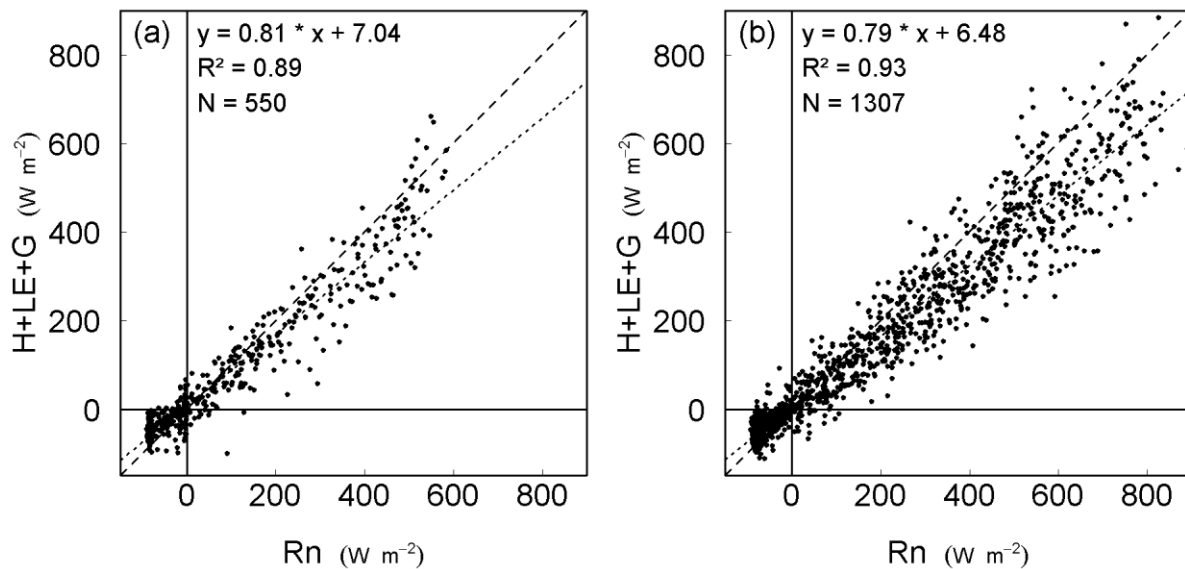


Figure S4. Energy balance closure at the turbulence tower during IOP-1 (left) and IOP-2 (right)

6. Local circulation systems

The aim of this section is to show the (potential) effect of the clear cut (south of the *Waldstein-Weidenbrunnen* site) on the flow in the roughness layer and its influence on trace gas concentrations. For stronger winds, the wind direction of the entire boundary layer dominates also down to the canopy level. In contrast, under light wind conditions (cloudy conditions), there are very small horizontal wind velocities above the canopy and significantly lower vertical wind velocities (not shown). Then the effect of the clear cut on the wind field of the site becomes obvious (see Fig. S5). In general, main wind directions – in the south-west sector – are nearly identical at 200 m (sodar) and 1050 m (windprofiler) heights. A strong SE component, coming up the Lehestenbach valley, could occur as well, but only below 100 m at night.

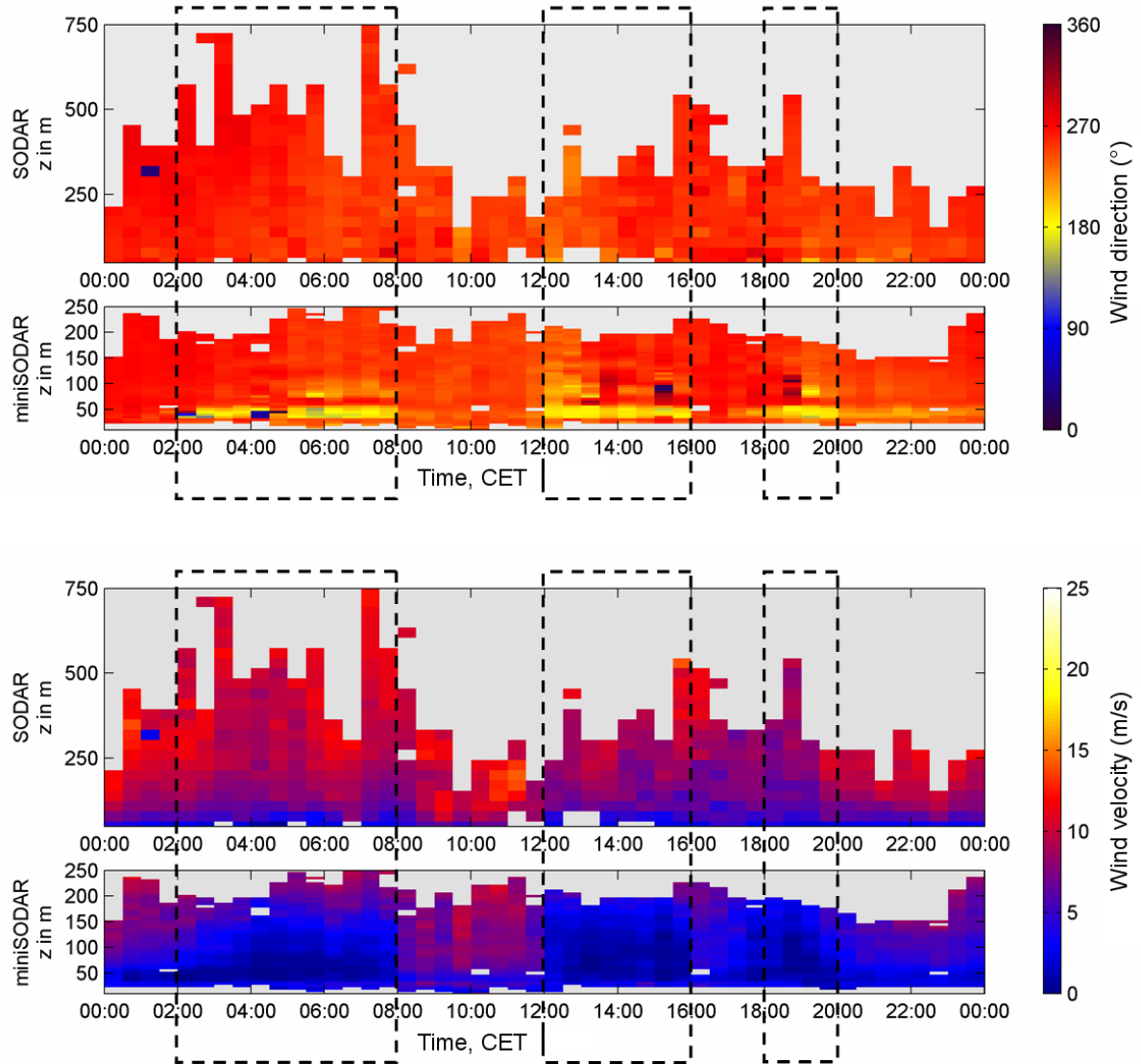


Figure S5. Time-height cross-sections from sodar and mini-sodar data of wind direction (above) and wind velocity (below) on June 28, 2008. Periods with southerly winds directly above the canopy (originating from the clear-cut) are highlighted.

Analysis of coherent structures was extended to the lower boundary layer according to Thomas et al. (2006) using sodar measurements. To derive characteristics of coherent structures from sodar/RASS individual soundings, data had to be preprocessed and wavelet analysis has to be applied. For occasional environmental noise detection and discarding of erroneous data, denoising and gap filling procedures were considered (Crescenti, 1998; Miller and Rochwarger, 1970; Neff and Coulter, 1986). Firstly, data were filtered using the error flag output by the sodar/RASS system. Secondly, a quality control tool, described in Thomas et al. (2006), was ap-

plied. Spectra of wavelet variance for different observation levels (14 September, 2007) are presented in Fig. S6. Data for the lower levels, which are comparable with corresponding structures responsible for the coupling, exhibit the first maximum at ~30 sec, whereas the higher observation levels show the stronger maximum at ~50-60 sec.

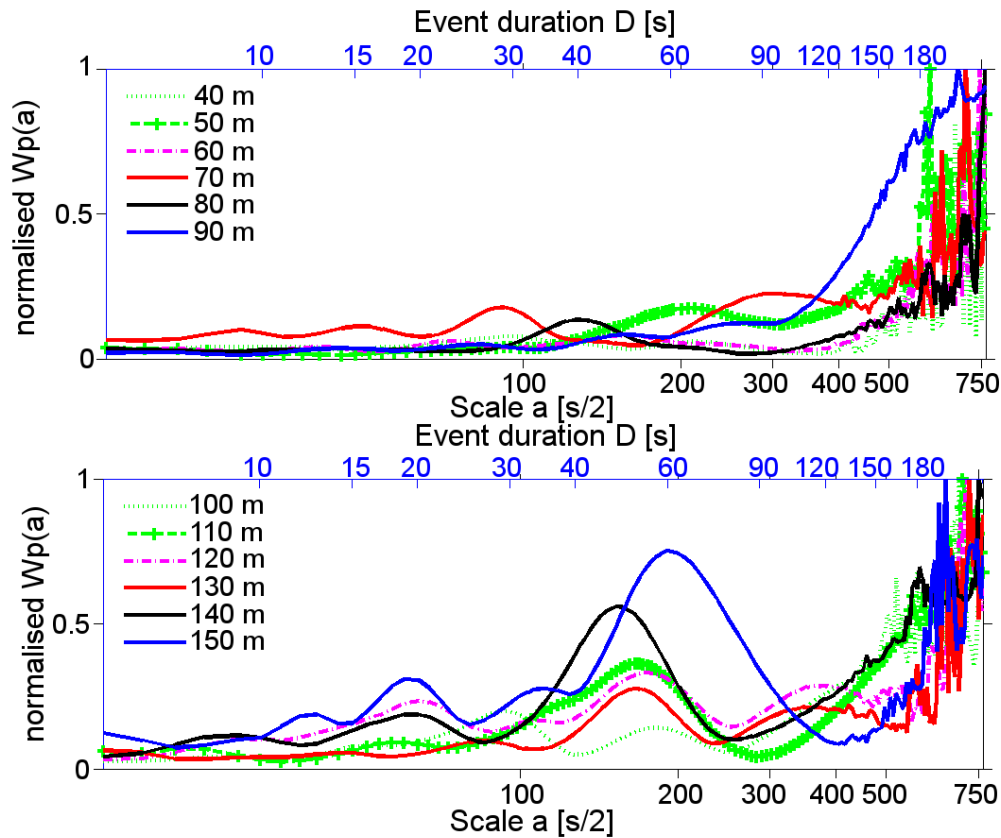


Figure S6. Normalized spectra of the wavelet variance of the vertical wind component at different observation levels during IOP-1 (14 September, 2007, 00:00 – 00:25 CET).

7. Time series of trace gas fluxes

Trace gas fluxes measured by the eddy covariance technique at 32 m above forest floor are shown in Fig. S7 (IOP-1: left panels, a–c; IOP-2: right panels, a–e). They comprise turbulent fluxes of water vapor (F_{H_2O}), carbon dioxide (F_{CO_2}), ozone (F_{O_3}), nitrogen dioxide (F_{NO_2}), nitric oxide (F_{NO}), and the composites $F_{O_x} = F_{O_3} + F_{NO_2}$ and $F_{NO_x} = F_{NO} + F_{NO_2}$. During the selected fair-weather days, F_{H_2O} clearly followed diel variations of available energy and H_2O gradients; it was close to zero during night, and up to 200 W m^{-2} during day (Fig. S7 a). Classic daily variations were found for F_{CO_2} , featuring negative fluxes during daytime (CO_2 up-

take by vegetation) and positive (respiration) fluxes during night (Fig. S7 b). As expected, ozone fluxes reflected during both IOPs the well-known O_3 deposition to forest vegetation and ground (Fig. 16 c, black symbols); F_{O_x} followed closely F_{O_3} (Fig. S7 c, grey symbols) for reasons explained below (see Section 3.5.). In contrast, F_{NO_2} (measured during IOP-2 only) was mostly directed upwards, with large fluxes during most of the daytime and smaller fluxes during night (Fig. S7 d, right panel). For NO, however, peaks of downward directed fluxes were determined during the morning hours, whereas F_{NO} was indistinguishable from zero for the rest of the day and also during night-time (Fig. S7 e, right panel).

Data gaps in F_{NO} and F_{NO_2} were due to routine calibration. The flux of the chemically conservative composite NO_x showed a very similar pattern to that of F_{NO_2} (Fig. S7 d, right panel, grey symbols), with the exception of those time periods between 06:00 and 12:00 CET, when F_{NO_x} was substantially lower than F_{NO_2} (due to noticeable $F_{NO} < 0$), which in turn is most likely the result of advection induced, strong and positive vertical gradients (downward) of NO concentration above the canopy. Otherwise, F_{NO_2} is approximately equal to F_{NO_x} , because the contribution of F_{NO} to F_{NO_x} is one order of magnitude lower than that of F_{NO_2} . Therefore, both F_{NO_x} and F_{O_x} (the flux of the chemically conservative composite $O_x = O_3 + NO_2$), and also the respective concentration differences, are not considered for the analysis of fluxes and concentration gradients vs. coupling stages (see Sect. 3.4 and 3.5).

The fluxes of $F_{NH_4^+,tot}$ and $F_{NO_3^-,tot}$ are shown in Fig. S7 (left panels, d and e) and were mostly directed downward to the forest canopy with pronounced diel variations. Wolff et al. (2010b) provide a detailed discussion about the magnitude of $F_{NH_4^+,tot}$ and $F_{NO_3^-,tot}$ with respect to comparable previous studies reported so far. Turbulent time scales (τ_{turb} , Eq. 2) for the surface layer above the canopy are also shown in Fig. S7 (panels f); they remained mostly below 50 s during both IOPs.

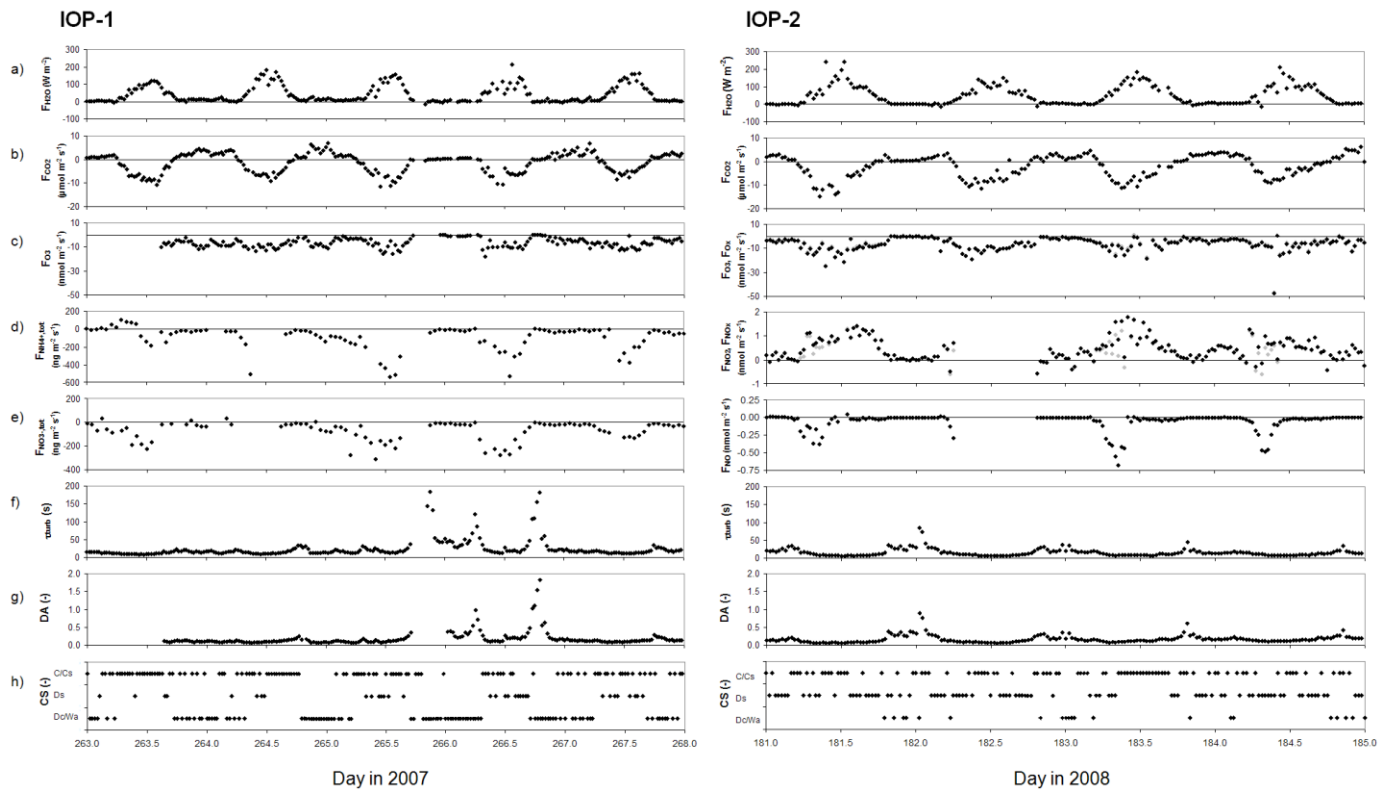


Figure S7. Results of flux measurements of gaseous and particulate trace compounds at the “main tower” during 20 – 24 September 2007 (IOP-1, DOY 263-267, left panels) and for 29 June to 02 July 2008 (IOP-2, DOY 181-184, right panels). (a) F_{H_2O} , (b) F_{CO_2} , (c) F_{O_3} (black symbols) and F_{O_x} (grey symbols, IOP-2 only), (d) $F_{NH_4^+,tot}$ (left panel) and F_{NO_2} and F_{NO_x} (right panel, black and grey symbols, respectively), (e) $F_{NO_3^-,tot}$ (left panel) and F_{NO} (right panel), (f) turbulent time scale τ_{turb} (24–32 m), (g) Damköhler number DA (24–32 m), (h) coupling regimes (determined from measurements at the ‘turbulence tower’, see section 3.1). Measurement heights were 32 m (a. gr.) for all fluxes measured by eddy covariance during IOP-1 (a–c), and during IOP-2 (a–e); fluxes of total ammonium and total nitrate (d and e, IOP-1), determined by aerodynamic gradient technique, refer to 27.1 m (geometric mean of the heights of both intake levels).

8. Time series of concentration differences between canopy top and forest floor

During both IOPs, H_2O concentration differences ($\Delta [H_2O] = [H_2O]_{24m} - [H_2O]_{0.9m}$) between the 24 m (canopy top) and 0.9 m (above understory) levels were for most of the daytime negative (upward), and positive during summertime nights (downward), confirming that we have observed well-known fair weather in-canopy gradients with moister conditions below the canopy compared to those above during day, and opposite gradients during night (Fig. S8 a). Most of the time, $\Delta [CO_2] = [CO_2]_{24m} - [CO_2]_{0.9m}$ was negative, however, during daytime it

was close to zero; highest CO₂ concentrations were found close to the forest floor at night (Fig. S8 b). As expected, $\Delta[\text{O}_3] = [\text{O}_3]_{24\text{m}} - [\text{O}_3]_{0.9\text{m}}$ was positive (downward) day and night during both IOPs, reflecting the well-known O₃ deposition to ground and vegetation (Fig. S8 c, black symbols). During the fall period (IOP-1), $\Delta[\text{NO}_2] = [\text{NO}_2]_{24\text{m}} - [\text{NO}_2]_{0.9\text{m}}$ exhibits a small diurnal course (negative during daytime, positive or close to zero during night, Fig. 19 d, left panel, black symbols); during most of the summer period (IOP-2), $\Delta[\text{NO}_2]$ was clearly negative (see Fig. S8 d, right panel, black symbols), once again indicating the already mentioned strong chemical source of NO₂ within the canopy. Gradients of NO_x(= NO₂+NO) between 24 m and 0.9 m (Fig. S8 d, grey symbols) show patterns very similar to those of NO₂, and gradients of O_x(= O₃+NO₂, Fig. S8 c, grey symbols) follow closely those of O₃. The latter is due to O₃ concentrations being one order of magnitude larger than NO₂ during the investigated time periods. Since the forest soil acts as a biogenic source of NO, $\Delta[\text{NO}] = [\text{NO}]_{24\text{m}} - [\text{NO}]_{0.9\text{m}}$ has actually been expected to be directed upward (i.e., negative, and presumably small). However, positive NO gradients (downward), particularly in the morning hours (06:00–12:00 CET), confirm the advective impact of traffic related NO sources (see Sect. 3.4), especially during IOP-1 (Fig. S8 e, left panel), but still visible in IOP-2, too (Fig. S8 e, right panel). Only for IOP-1, $\Delta[\text{HONO}] = [\text{HONO}]_{24\text{m}} - [\text{HONO}]_{0.9\text{m}}$ is available (Sörgel et al., 2011). During many of the daytime hours, $\Delta[\text{HONO}]$ was negative (upward) or close to zero, but positive (downward) during much of the night (Fig. S8 f).

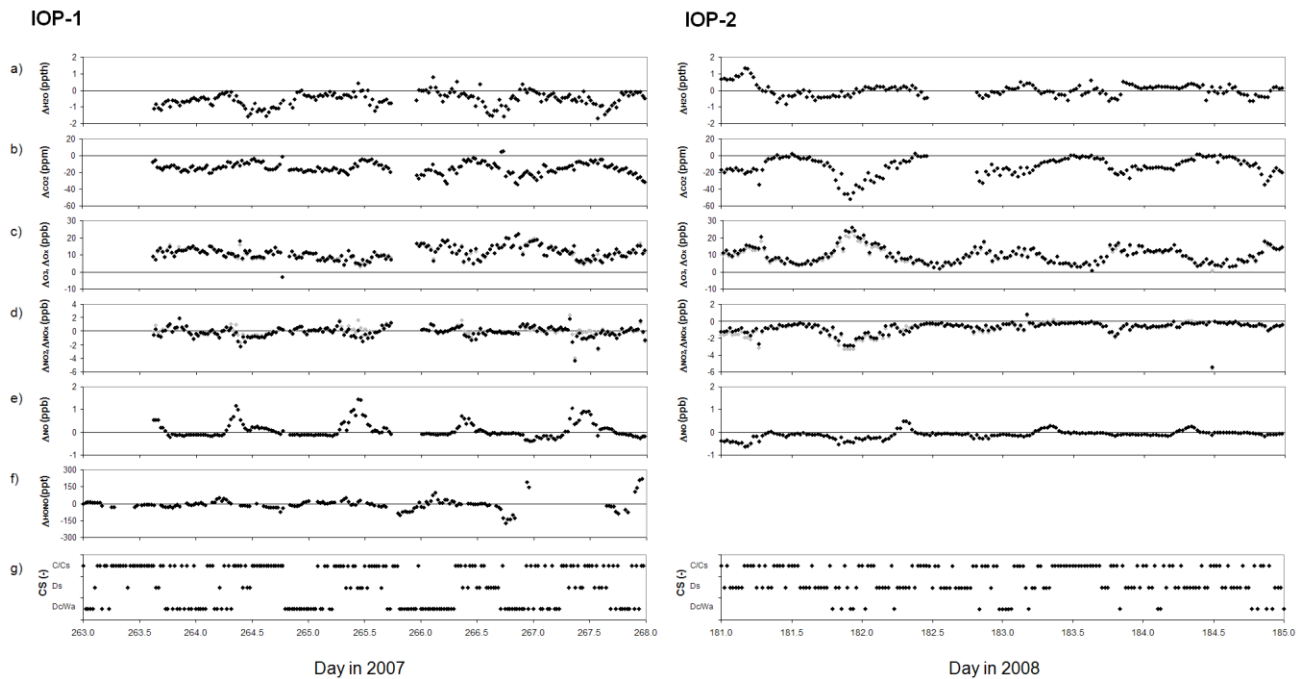


Figure S8. Concentration differences $\Delta[C] = [C]_{24m} - [C]_{0.9m}$ between the 24 m and the 0.9 m level at the ‘main tower’ for 20–24 September 2007 (IOP-1, DOY 263-267, left panels), and for 29 June to 2 July 2008 (IOP-2, DOY 181-184, right panels): (a) $\Delta[H_2O]$, (b) $\Delta[CO_2]$, (c) $\Delta[O_3]$ and $\Delta[O_x]$ (black and grey symbols, respectively), (d) $\Delta[NO_2]$ and $\Delta[NO_x]$ (black and grey symbols, respectively), (e) $\Delta[NO]$, (f) $\Delta[HONO]$ (IOP-1 only); (g) coupling regimes (determined from measurements at the ‘turbulence tower’, see Sect. 3.1). Note that a positive concentration difference indicates a downward, while a negative concentration difference an upward directed concentration gradient.

9. References

Atkinson, R., Baulch, D. L., Cox, R. A., Crowley, J. N., Hampson, R. F., Hynes, R. G., Jenkin, M. E., Rossi, M. J., and Troe, J.: Evaluated kinetic and photochemical data for atmospheric chemistry: Volume I - gas phase reactions of O_x , HO_x , NO_x and SO_x species, *Atmos. Chem. Phys.*, 4, 1461-1738, 10.5194/acp-4-1461-2004, 2004.

Aubinet, M., Grelle, A., Ibrom, A., Rannik, Ü., Moncrieff, J., Foken, T., Kowalski, A. S., Martin, P. H., Berbigier, P., Bernhofer, C., Clement, R., Elbers, J., Granier, A., Grünwald, T., Morgenstern, K., Pilegaard, K., Rebmann, C., Snijders, W., Valentini, R., and Vesala, T.: Estimates of the annual net carbon and water exchange of forests: The EUROFLUX methodology, *Adv. Ecol. Res.*, 30, 113-175, 2000.

Cellier, P., and Brunet, Y.: Flux-gradient relationships above tall plant canopies, *Agric. Forest. Meteorol.*, 58, 93-117, 1992.

Crescenti, G.: The degradation of Doppler sodar performance due to noise: A review, *Atmos. Environm.*, 32, 1499-1509, 1998.

Dlugi, R.: Interaction of NO_x and VOC's within vegetation, in: Proceedings EUROTRAC-Symposium 92, edited by: Borrell, P. W., SPB Acad. Publ., The Hague, 682-688, 1993.

Eigenmann, R., Metzger, S., and Foken, T.: Generation of free convection due to changes of the local circulation system, *Atmos. Chem. Phys.*, 9, 8587-8600, 2009.

Foken, T.: Climate change in the Lehstenbach region, in: Biogeochemistry of Forested Catchments in a Changing Environment, A German Gase Study. Ecological Studies, edited by: Matzner, E., Springer, Berlin, Heidelberg, 59-66, 2004.

Foken, T.: *Micrometeorology*, Springer, Berlin, Heidelberg, 308 pp., 2008a.

Foken, T.: The energy balance closure problem - An overview, *Ecolog. Appl.*, 18, 1351-1367, 2008b.

Garratt, J. R.: *The atmospheric boundary layer*, Cambridge University Press, Cambridge, 316 pp., 1992.

Kottek, M., Grieser, J., Beck, C., Rudolf, B., and Rubel, F.: World Map of the Köppen-Geiger climate classification updated, *Meteorol. Z.*, 15, 259-263, 2006.

Lenschow, D. H.: Reactive trace species in the boundary layer from a micrometeorological perspective, *J. Meteor. Soc. Japan*, 60, 472-480, 1982.

Lüers, J., Foken, T., Grasse, B., and Döbele, T.: Jahresbericht 2008 zum Förderprojekt 01879, Untersuchung der Veränderung der Konzentration von Luftbeimengungen und Treibhausgasen im hohen Fichtelgebirge, *Arbeitsergebn.*, Univ. Bayreuth, Abt. Mikrometeorol., ISSN 1614-89166, 39, 25 pp., 2009.

Mayer, J. C., Bargsten, A., Rummel, U., Meixner, F. X., and Foken, T.: Distributed Modified Bowen Ratio method for surface layer fluxes of reactive and non-reactive trace gases, *Agric. Forest. Meteorol.*, 151, 655-668, 2011.

Miller, K., and Rochwarger, M.: On estimates of spectral moments in the presence of colored noise, *IEEE Trans. Inf. Theory*, 16, 303-308, 1970.

Mölder, M., Grelle, A., Lindroth, A., and Halldin, S.: Flux-profile relationship over a boreal forest - roughness sublayer correction, *Agric. Forest. Meteorol.*, 98-99, 645-648, 1999.

Monteith, J. L., and Unsworth, M. H.: *Principles of environmental physics*, 3rd edition, Elsevier, Academic Press, Amsterdam, Boston, 418 pp., 2008.

Neff, W., and Coulter, R. L.: Acoustic Remote Sensing, in: *Probing the atmospheric boundary layer*, edited by: Lenschow, D. H., American Meteorological Society, Boston, 201-239, 1986.

Seifert, W.: Klimaänderung und (Winter-) Tourismus im Fichtelgebirge - Auswirkungen, Wahrnehmung und Ansatzpunkte zukünftiger touristischer Entwicklung, Fakultät für Biologie, Chemie und Geowissenschaften, Universität Bayreuth, Bayreuth, 206 + XL pp., 2004.

Siebicke, L.: Footprint synthesis for the FLUXNET site Waldstein/Weidenbrunnen (DE-Bay) during the EGER experiment, *Arbeitsergebn.*, Univ. Bayreuth, Abt. Mikrometeorol., ISSN 1614-89166, 38, 45 pp, 2008.

Sörgel, M., Trebs, I., Serafimovich, A., Moravek, A., Held, A., and Zetzsch, C.: Simultaneous HONO measurements in and above a forest canopy: Influence of turbulent exchange on mixing ratio differences, *Atmos. Chem. Phys.*, 11, 841-855, 2011.

Thomas, C., Mayer, J.-C., Meixner, F. X., and Foken, T.: Analysis of the low-frequency turbulence above tall vegetation using a Doppler sodar, *Boundary-Layer Meteorol.*, 119, 563-587, 2006.

Wolff, V., Trebs, I., Ammann, C., and Meixner, F. X.: Aerodynamic gradient measurements of the NH_3 - HNO_3 - NH_4NO_3 triad using a wet chemical instrument: an analysis of precision requirements and flux errors, *Atmos. Meas. Techn.*, 3, 187-210, 2010a.

Wolff, V., Trebs, I., Foken, T., and Meixner, F. X.: Exchange of reactive nitrogen compounds: concentrations and fluxes of total ammonium and total nitrate above a spruce canopy, *Biogeosci.*, 7, 1729–1744, 2010b.

Wulfmeyer, V., Behrendt, A., Kottmeier, C., Corsmeier, U., Barthlott, C., Craig, G., Hagen, M., Althausen, D., Aoshima, F., Arpagaus, M., Bauer, H. S., Bennett, L., Blyth, A., Brandau, C., Champollion, C., Crewell, S., Dick, G., Di Girolamo, P., Dorninger, M., Dufournet, Y., Eigenmann, R., Engelmann, R., Flamant, C., Foken, T., Gorgas, T., Grzeschik, M., Handwerker, J., Hauck, C., Höller, H., Junkermann, W., Kalthoff, N., Kiemle, C., Klink, S., König, M., Krauß, L., Long, C. N., Madonna, F., Mobbs, S., Neininger, B., Pal, S., Peters, G., Pigeon, G., Richard, E., Rotach, M., Russchenberg, H., Schwitalla, T., Smith, V., Steinacker, R., Trentmann, J., Turner, D. D., van Baelen, J., Vogt, S., Volkert, H., T., W., Wernli, H., Wieser, A., and Wirth, M.: The convective and orographically induced precipitation study (COPS): The scientific strategy, the field phase, and research highlights, *Quart. J. Roy. Meteorol. Soc.*, 137, 3-30, 2011.